Seismic Characterization of Wind Turbine Sites Near Lawton, Oklahoma, by the MASW Method

Choon B. Park and Richard D. Miller

Kansas Geological Survey
University of Kansas
1930 Constant Avenue
Lawrence, Kansas 66047-3726

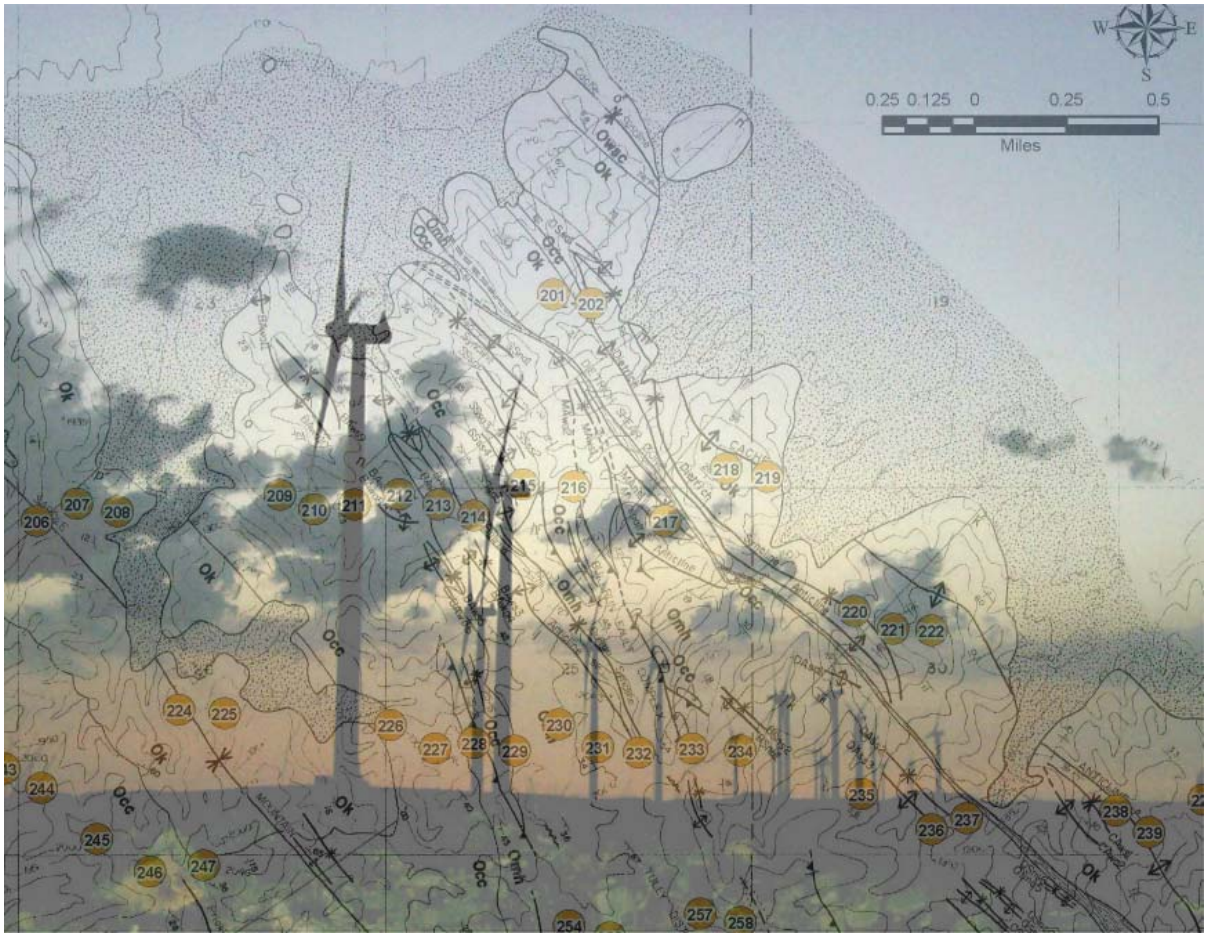

Final Report to

Rick Palm and Chris Kopchynski
Barr Engineering Company
4700 West 77th Street
Minneapolis, MN 55435-4803

Open File Report 2005-22 (part 1 of 4) July 5, 2005

Contents at a Glance

Page

PROJECT DESCRIPTION ---------- 2-5

Summary
General Acquisition Parameters and Site Descriptions
Field Logistics for Vs, SSA, and SIA Analyses
Data Processing for 2-D Analyses and Voids Interpretations

DESCRIPTION OF METHODS USED ---------- 5-9

General Procedure with MASW Method for 1-D Vs Profile
Key Acquisition Parameters for 1-D Vs Profile
2-D Shear-Wave Velocity (Vs) Mapping
Side Scattering Analysis (SSA)
Surface-Wave Imaging by Attenuation (SIA)

ACKNOWLEDGMENTS ---------- 10

REFERENCES ---------- 10

TABLES ---------- 11-15

Table 1: Average Vs at all eighty-four (84) turbine sites in Blue Canyon Phase II
Table 2: Summary table of potential voids (Blue Canyon Wind Mill Farm Phase II)
Table 3: Sites where one or more lines were adjusted to a shorter length due to terrain conditions
Table 4: Optimum acquisition parameters—Rules of thumb

FIGURES ---------- 16-27

APPENDICES

APPENDIX I: 2-D Maps from Shear-Wave Velocity (Vs) Analysis
APPENDIX II: 2-D Maps from Side Scattering Analysis (SSA)
APPENDIX III: 2-D Maps from Surface-Wave Imaging by Attenuation (SIA)

Seismic Characterization of Wind Turbine Sites Near Lawton, Oklahoma, by the MASW Method

The performed project is described first and then those seismic surface-wave methods used for the project are explained later.

PROJECT DESCRIPTION

Summary

The multichannel analysis of surface waves (MASW) method (Park et al., 1999) was applied to a total of eighty-four (84) turbine sites planned for the second phase construction in the Blue Canyon Wind Mill Farm (Figure 1) near Lawton, Oklahoma, for seismic characterization of the upper 15 m or so of ground materials. The main purposes of the project were a) to evaluate ground stiffness as deduced from shear-wave velocity (Vs), and b) to estimate the potential existence of weak zones such as voids and fractured areas for the volume of ground materials defined by 100 ft (x-width) x 100 ft (y-width) x 50 ft (z-depth) volumes.

All eighty-four (84) sites were surveyed for the 2-D Vs evaluation that generated 2-D Vs maps showing both lateral and vertical change in Vs. In addition, a unique surface-wave method was also applied to each site to delineate subsurface anomalies by their surface (x and y) coordinates. This method is called "Side Scattering Analysis (SSA)" because its principles are based on the utilization of surface waves scattered from an anomaly sideways with respect to the seismic-survey lines. Multiple 2-D Vs maps were obtained because this SSA method required multiple seismic-survey lines deployed in a 2-D (*x* and *y*) format with data acquisition of each line identical to that for the 2-D Vs mapping. This increased the reliability and utility of the Vs evaluation provided by the redundant spatial sampling. Both 2-D Vs maps and SSA maps were used to interpret anomalies. As a supplementary tool a method called surface-wave imaging by attenuation (SIA) (Park et al., 1998a) was also used to help interpret anomalies by applying it to the same shot records used for 2-D Vs mapping.

For the interpretation of anomalies, any localized zone of anomalously low Vs in the 2-D Vs maps was first identified and then cross checked for possible back-scattering features on the corresponding seismic-shot records. Localized accumulations (or troughs) of amplitude in the SSA maps were also interpreted as potential anomalies. Effectiveness of SIA analysis to interpret anomalies was marginal.

A testing survey was made at one of the turbine sites on March 29 to evaluate optimum acquisition parameters. Then, production surveys were performed during the period of April 13-June 9, 2005, for a total of thirty-one (31) field days operated by a three (3)-person (on the average) crew.

Vs in the area as indicated by the 2-D Vs analysis changed from about 700 m/sec within the uppermost 5-m depth range to about 1000 m/sec at a depth range of 10 m, and then to about 1400 m/sec at deeper depths down to maximum investigation depth of approximately 20 m or so (Table 1). Within this range, however, each site showed different patterns of Vs variation

in both vertical and lateral directions. A total of sixty-nine (69) anomalies were interpreted as potential voids from the 2-D Vs, SSA, and SIA analyses (Table 2). Final 2-D Vs, SSA, and SIA maps for all 84 sites are presented with interpretations of voids in separate volumes of Appendices I, II, and III, respectively.

In this report, each surveyed site is denoted by the assigned turbine-tower number. For example, the site of turbine-tower number 201 is denoted by T-201, and T-001 is the site of turbine-tower number 1. The fundamental mode of surface waves is to be denoted by M0, and higher modes are denoted by M1 (the first higher mode), M2 (the second higher mode), and so on.

General Acquisition Parameters and Site Description

A 24-channel Geometrics Geode was used as the main recording device. Two units were used to form a 48-channel acquisition system. One 4.5-Hz geophone was used as receiver at each station whose interval was 4 ft. A total recording time of 1000 ms (1 sec) was used with a 1-ms sampling interval. No acquisition filters were used.

Surface condition of the area was rough in general with a thin (or no) layer of soil and rocks of a few feet size scattered within the surveying boundary (Figure 2). Geophone locations were sometimes moved by several inches from the exact designed points to find those spots with enough soil for planting. Whenever these spots could not be located within maximum one foot from the designed spot, they were laid sideways on top of the surface without the spike coupling. Although corresponding seismic traces should look different with weaker energy than others of normal coupling, their influence on the surface-wave dispersion processing is usually insignificant.

Field Logistics for Vs, SSA, and SIA Analyses

At each site, four survey lines were laid out according to the logistics schematically illustrated in Figure 3. Line 1 crossed the location of the tower center from north to south, whereas lines 2-4 crossed northern, center, and southern parts of the 100 ft x 100 ft tower boundary from east to west. The bearing of each line was assisted by using a Brunton Compass. Each line consisted of forty-eight (48) receiver stations of 4.5-Hz geophones (starting from grid number 23 as indicated in Figure 3), and two 24-channel Geometrics Geode seismographs were connected together to acquire 48-channel shot records. The first shot point was located two stations (8 ft) away (grid number 25) from the first (channel #1) geophone location. Three impacts were delivered at each shot station and vertically stacked to make one shot record. A total of twenty-four (24) shot records were acquired with each survey line by continuously moving shot points to the next station, ending at grid number 2. During the processing stage these twenty-four 48-channel records were then recompiled to simulate the 24-channel roll-along acquisition mode. A total of ninety-six (96) shot records were acquired at each site. Each record was assigned a unique file name consisting of site number plus the shot sequence number (for example, the first record at T-245 was named as "24501.dat"). Summary of acquisition parameters is also listed in Figure 3.

At some sites (16 sites total), one or more survey lines (out of four) had to be adjusted to a shorter length by using a shorter receiver spacing of 2 ft due to a limited space available for the survey (Table 3).

Data from all four lines were used to generate 2-D Vs and SIA maps, four of each type, and those from lines 2 and 4 were used to generate an SSA map.

Data Processing for 2-D Analyses and Voids Interpretations

The following data-processing sequence was used for the 2-D analyses (Vs, SSA, and SIA):

1. Converting all shot record files from SEG-2 to KGS format
2. Decimating every other sample to reduce total number of samples per record
3. Encoding source and receiver locations in x-y coordinates (see Figure 3)
4. Compiling into separate files of 24-channel roll-along acquisition mode for lines 1-4
5. Analyzing dispersion curves for each line (maximum twenty-four [24] dispersion curves generated for each line)
6. Inversion to generate 2-D Vs maps (total four maps generated per site)
7. Selecting a reference dispersion curve for SSA processing (usually the curve obtained from the record whose receiver spread was centered at the tower center in line 1)
8. Generating one SSA map
9. Generating four (lines 1-4) SIA maps using the same reference dispersion curve used for SSA analysis.

Quality of the surface-wave data is judged from the quality of dispersion trend observed in a transformed wavefield space called the overtone image (Park et al., 1998b). Typical quality of seismic records collected in the area is displayed in Figure 4a. Most of energy was focused in the frequency range of 20-70 Hz with phase velocities changing within 1000-2000 m/sec. This trend was then usually followed by another trend of much weaker energy and lower velocities (< 1000 m/sec) at the higher frequencies (70-230 Hz) with little change in phase velocity. It is believed that this lower-velocity trend with little change was originating from the uppermost (a few meters) rock layer most influenced by the weathering process. Figure 4b shows an example of the highest-quality records that constitute less than a few percent of total records. Some records had such a poor quality that no dispersion trend could be identified and they were discarded (Figure 4c). Missing marks at the bottom of the final 2-D Vs map indicate the surface locations (midpoint of the receiver spread used) of these discarded records (Figure 5). This type of record constituted about five (5) percent of total records acquired.

Dispersion curves were first automatically extracted by using an algorithm that follows the energy trends and then manually edited by discarding those outliers not fitting into a reasonable trend and also by adding those points that could not be automatically picked due to weak energy. Most of the extracted curves were in the frequency range of 30-200 Hz with the phase velocities in 500 m/sec – 2000 m/sec. Inversion of the extracted dispersion curves was performed using the algorithm by Xia et al. (1999). A ten-varying-thickness layer model was created at the beginning of the inversion with the maximum depth (Z_{max}) (top of the half

space) being about 30% of the longest wavelength. Z_{max} was usually in the range of 20-30 m. Initial Vs model was created with the aid of phase velocity versus wavelength relationship depicted by the dispersion curve. Poisson's ratio of 0.3 and density of 2.0 gr/cc were assigned for all ten layers during the inversion process. The iterative inversion was forced to stop after the fifth iteration of updating the Vs model. This relatively small number of iterations was chosen to minimize the effect of computational artifacts.

Side Scattering Analysis (SSA) was applied to records of lines 2 and 4 by using a reference dispersion curve for a square (20 m x 20 m) surface (x and y) area (Figure 6) with a grid interval of 0.2 m. The reference dispersion curve was chosen among those obtained near the tower center that had an M0 curve best defined for wavelengths shorter than 20 m so that the depth of sensitivity was focused into 0-10 m.

Surface-wave Imaging by Attenuation (SIA) analysis was applied to records of all four lines (lines 1-4) by using another reference curve chosen among those near the tower center that had the greatest range of wavelengths so that the sensitivity depth could be maximized. One 2-D map was obtained from records of one seismic line, totaling four maps per site.

To interpret anomalies, first any localized zone of anomalously low velocities in the 2-D Vs maps was identified and then cross checked for possible back-scattering features on the corresponding seismic-shot records. Localized accumulations (or troughs) of amplitude in the SSA maps were also interpreted as potential anomalies. Effectiveness of the SIA analysis to interpret anomalies was marginal. A total of sixty-nine (69) anomalies were interpreted as potential voids from the 2-D Vs, SSA, and SIA analyses. A summary of interpreted anomalies (voids) is listed in Table 2. Final 2-D Vs, SSA, and SIA maps for all 84 sites are presented with interpretations of voids in separate volumes of Appendices I, II, and III, respectively. Vs values obtained from all four lines at each site were averaged for top 5 m, 10 m, and 20 m depth ranges, respectively. These values are listed in Table 1 and represented in a chart format in Figure 7. Also, average Vs values from N-S line (line 1) and E-W lines (lines 2-4) were separately obtained for a possible study of seismic anisotropy in association with any regional lineation features in the area.

DESCRIPTION OF METHODS USED

Detailed description of the theory of the multichannel analysis of surface waves (MASW) method and typical field application can be found in Park et al. (1999), Xia et al. (1999), and Miller et al. (1999).

General Procedure with MASW Method for 1-D Vs Profile

A multiple number of receivers (usually 24 or more) are deployed with even spacing along a linear survey line with receivers connected to a multichannel recording device (seismograph) (Figure 8). Each channel is dedicated to recording vibrations from one receiver. One multichannel record (commonly called a shot gather) consists of a multiple number of time series (called traces) from all the receivers in an ordered manner.

Data processing consists of three steps (Figure 9): 1) preliminary detection of surface waves, 2) constructing the dispersion image panel and extracting the signal dispersion curve, and 3) back-calculating Vs variation with depth. All these steps can be fully automated. The preliminary detection of surface waves examines recorded seismic waves in the most probable range of frequencies and phase velocities. Construction of the image panel is accomplished through a 2-D (time and space) wavefield transformation method that employs several pattern-recognition approaches (Park et al., 1998b). This transformation eliminates all the ambient cultural noise as well as source-generated noise such as scattered waves from buried objects (building foundations, culverts, boulders, etc.). The image panel shows the relationship between phase velocity and frequency for those waves propagated horizontally and directly from the impact point to the receiver line. These waves include fundamental and higher modes of surface waves as well as direct (compressional) body waves (Figure 9b). The necessary dispersion curve, such as that of fundamental-mode Rayleigh waves, is then extracted from the energy accumulation pattern in this image panel (Figure 9b). The extracted dispersion curve is finally used as a reference to back-calculate the Vs variation with depth below the surveyed area. This back-calculation is called inversion and the process can be automated with reasonable constraints (Xia et al., 1999).

Key Acquisition Parameters for 1-D Vs Profile

Unlike other seismic methods (e.g., reflection or refraction), acquisition parameters for MASW surveys have quite a wide range of tolerance. This is because the multichannel processing schemes employed in the wavefield transformation method (Park et al., 1998b) have the capability to automatically account for such otherwise adverse effects as near-field, far-field, and spatial aliasing effects (Park et al., 1999). Nevertheless, two types of parameters are considered to be most important: the source offset (x_1) and the receiver spacing (dx) (Figure 8). The source offset (x_1) needs to change in proportion to the maximum investigation depth (z_{max}). A conservative rule of thumb would be $x_1 = \gamma z_{max}$ with γ=0.5. However, very often γ can be as small as 0.1 (Park et al., 1999). The receiver spacing (dx) may need to be slightly dependent on the average stiffness of near-surface materials. A rule of thumb is $dx \approx 1.0$ m in most surveys over soil sites. Table 4 summarizes optimum ranges of all the acquisition parameters (Park et al., 2002).

2-D Shear-Velocity (Vs) Mapping

A 2-D Vs map is constructed from the acquisition of multiple records (Figure 10) with a fixed source-receiver configuration and a fixed increment (dC) of the configuration (Figure 11). A source-receiver configuration indicates a setup of given source offset (x_1), receiver spacing (dx), and total number of channels (N) used during a survey. The increment dC depends on the degree of horizontal variation in Vs along the entire survey line (Park, 2005). A small increment would be necessary if a high degree of horizontal variation is expected. In most cases where total receiver spread length (x_T) is set in such a way that horizontal variation within x_T can be ignored, an increment of half the spread would be sufficient: $dC \approx 0.5\, x_T$. Therefore, determination of optimum x_T has to be made before optimum dC is determined. In theory, a shorter x_T would ensure a higher accuracy in handling the horizontal variation. However, it would also impede the accurate assessment of dispersion curves (Park

et al., 2001). Therefore, there is a trade-off. In most soil-site applications, x_T in the range of 10-30 m is most optimal and this gives an optimal *dC* in the range of 5-15 m.

Once multiple records (> 5) are acquired by regularly moving the source-receiver configuration, one 1-D Vs profile is obtained from each record through the surface-wave processing outlined previously. Each Vs profile also has the appropriate horizontal coordinate (i.e., station number) to represent the vertical Vs variation. Naturally, the midpoint of the receiver spread is used for this purpose. Multiple 1-D Vs profiles obtained are then used for a 2-D (*x* and *z*) interpolation to create the final 2-D map (Figure 10).

Side Scattering Analysis (SSA)

Surface waves are known to be sensitive to the presence of near-surface anomalies such as near-vertical fractures and voids. A significant amount of surface wave energy impinging against them is transformed into scattered surface waves due to anomalies acting as new sources of surface waves (Figure 12). Therefore, MASW data collected for normal 2-D Vs mapping can also be used to detect possible anomalies existing subsurface off the survey line by using a processing scheme similar to the conventional reflection processing. This process is called a side-scattering analysis (SSA) of surface waves. A brief explanation of the processing scheme follows.

When a void exists below a certain surface location (x_v, y_v), then a scattered surface-wave component of *f*-Hz traveling with a phase velocity of C_f generated by impact of a source located at (x_s, y_s) will reach a receiver point (x_r, y_r) at time $\delta t(f)$ (Figure 13):

$$\delta t(f) = \left(L_1 + L_2\right) / C_f \tag{1}$$

with $L_1 = \sqrt{\left(x_s - x_v\right)^2 + \left(y_s - y_v\right)^2}$ and $L_2 = \sqrt{\left(x_r - x_v\right)^2 + \left(y_r - y_v\right)^2}$

Based on this travel-time relationship, to evaluate the relative probability of a surface point being the source of such scattering, a plane (*x*-*y*) grid is first established within which the detection of subsurface anomalies is sought (Figure 13). Then, each point (x_v, y_v) in the grid is assumed to be the source of scattering. The corresponding scattered wavefields are then collapsed to their origin in time by applying an appropriate phase shift and then all those collapsed waves are summed (stacked) together to yield an indicator $SSA(x_v, y_v)$:

$$SSA(x_v, y_v) = \left| \sum_{\text{traces}} \sum_{\text{frequencies}} e^{-j2\pi f \delta t(f)} R_{r,s}^{Norm}(jf) \right|, \tag{2}$$

where $R_{r,s}^{Norm}(jf)$ indicates the normalized Fourier transformation of seismic trace $r_s(t)$ recorded by the receiver at (x_r, y_r) when seismic source was located at (x_s, y_s). *SSA* is proportional to the intensity of scattering, therefore qualitatively the existence probability of an anomaly. Therefore, when these values of SSAs calculated at all the grid points are displayed through a simple 2-D format, actual points of scattering will show peaks or troughs depending on whether there is a 180° phase shift at the time of scattering or not (Figure 14).

In the modeling illustration in Figure 14, the 180° phase shift was assumed. Phase velocities (C_f's) of a dispersion curve representative of the area are used in the calculation of $\delta t(f)$. The depth range sensitive to this analysis is assumed to be half the range of wavelengths defined by the representative dispersion curve. For example, if the reference curve has phase velocities changing from 1000 m/sec at the lowest frequency of 20 Hz to 100 m/sec at the highest frequency of 100 Hz, then corresponding wavelengths change from 50 m to 1 m and the sensitive depth range of the SSA analysis becomes 25 m – 0.5 m.

Sensitive depth range of SSA method is expected to be about the half the wavelengths used during the processing and the sensitive dimension (in diameter) of anomaly is expected to be about 10 % of its depth of existence. For example, if the reference curve had wavelengths in 4-20 m, then depth (z) of 2-10 m is sensitive for those anomalies larger than 0.2 m existing at z = 2 m, 0.5 m existing at z = 5 m, and so on.

More details of this processing scheme will be available in near-future publications.

Surface-Wave Imaging by Attenuation (SIA)

A near-surface anomaly is defined here as that part of near-surface materials that have elastic properties significantly different from the surrounding study area. The transition from normal zone to anomaly zone may be either abrupt or gradual.

During a surface wave survey, a near-surface anomaly will leave a signature of its presence on multichannel records in several forms. The most common signature is different phase velocities for those frequencies propagating through or near the anomaly. Another form would be different attenuation characteristics.

Besides different phase velocities and attenuation characteristics, an anomaly may reveal its presence through the generation of higher modes and reflected and diffracted surface waves. Generation of the higher modes becomes significant, especially in the case of velocity inversion and when energy of the higher modes tends to increase for high frequencies (Tokimatsu et al., 1992). Reflected and diffracted ground roll will be generated if the transition from normal zone to anomaly zone is abrupt. All these types of anomaly signatures may appear on a multichannel record when either the source or receivers are located at or near the surface location of the anomaly.

Theoretically, surface waves cannot penetrate a void filled with air or fluid because of the lack of shear modulus inside the void. However, the bulk of mass experiencing the retrograde elliptical motion of surface waves increases as penetration depth increases. Therefore, surface waves with penetration depths greater than or comparable to the depth of the void will experience certain changes in either attenuation or phase velocity, or both. Based on the outlined principles, the data processing scheme for SIA analysis is briefly explained below.

Dynamic linear move out (DLMO) correction is applied to each shot gather to correct for the offset effect, therefore, to flatten the linearly sloping events of surface waves (Park et al.,

1996). The correction is a dynamic operation because the amount of correction changes with time as well as offset. DLMO can be accomplished in the frequency domain as follows:

$$W_{DLMO}(f,x) = e^{j\Phi_f} W(f,x), \tag{3}$$

where

$W(f,x)$ = Fourier transform applied to time axis of a shot gather, $w(t,x)$,
$W_{DLMO}(f,x)$ = Fourier transform of DLMO-corrected shot gather, $w_{DLMO}(t,x)$,
x = distance from source,
Φ_f = $2\pi fx/C_f$, and
C_f = phase velocity for frequency *f*.

The velocity function C_f used in DLMO correction is calculated from a shot gather obtained at a reference location. The reference location is a presumably normal zone within the survey line. All traces in a DLMO-corrected shot gather are then stacked together to produce one stacked trace per shot.

After stacking, this procedure achieves the following:

- Those frequencies that have phase velocity equivalent to that at the reference location will have large stacked amplitudes through constructive interference.
- For those shot gathers obtained at or near the surface location of an anomaly, DLMO correction will result in stacked traces of weak amplitudes through destructive interference for those frequencies that have penetration depths comparable to the depth of the anomaly.
- All the higher modes will be attenuated through destructive interference because of their different phase velocities.
- All nonplanar, reflected, and diffracted ground rolls (and possibly any body-wave events) will be attenuated through destructive interference because of their nonlinear occurrence on a multichannel record.
- Random noise will be attenuated.

When stacked traces are displayed, all the normal zones will show large amplitudes and the anomalous zones will be denoted by attenuated amplitudes (Figure 15). The degree of attenuation will be proportional to the degree of being anomalous with respect to the reference location. Although a systematic study has not been performed yet, the sensitivity of the SIA method is expected to be much lower than that of the SSA method.

More detailed description of SIA analysis can be found in Park et al. (1998a).

ACKNOWLEDGMENTS

We would like to thank Ray Bragg and Kevin McClay from Mortenson Construction Company for their assistance during the field operations. Our sincere appreciation goes to many people involved in the preparation and the operation of field surveys; among them are David Thiel, Andrew Newell, and Nicolette Proudfoot. Also, David Laflen, Brett Bennett, and Mary Brohammer at the Kansas Geological Survey played critical roles in the background making necessary arrangements.

REFERENCES

Miller, R.D., Xia, J., Park, C.B., and Ivanov, J., 1999, Multichannel analysis of surfaces waves to map bedrock: *The Leading Edge*, v. 18, no. 12.

Park, C.B., 2005, MASW—Horizontal resolution in 2-D shear-wave velocity (Vs) mapping: Kansas Geological Survey, Open-file Report 2005-4.

Park, C.B., Miller, R.D., and Miura, H., 2002, Optimum field parameters of an MASW survey [Exp. Abs.]: SEG-J, Tokyo, May 22-23, 2002.

Park, C.B., Miller, R.D., and Xia, J., 2001, Offset and resolution of dispersion curve in multichannel analysis of surface waves (MASW): Proceedings of the SAGEEP 2001, Denver, Colorado, SSM-4.

Park, C.B., Miller, R.D., and Xia, J., 1999, Multi-channel analysis of surface waves (MASW): *Geophysics*, v. 64, no. 3, p. 800-808.

Park, C.B., Miller, R.D., and Xia, J., 1998a, Ground roll as a tool to image near-surface anomaly [Exp. Abs.]: Soc. Explor. Geophys., p. 874-877.

Park, C.B., Miller, R.D., and Xia, J., 1998b, Imaging dispersion curves of surface waves on multi-channel record [Exp. Abs.]: Soc. Explor. Geophys., p. 1377-1380.

Park, C.B., Miller, R.D., and Xia, J., 1996, Multi-channel analysis of surface waves using Vibroseis (MASWV) [Exp. Abs.]: Soc. Explor. Geophys., p. 68-71.

Tokimatsu, K., Tamura, S., and Kojima, H., 1992, Effects of multiple modes on Rayleigh wave dispersion characteristics: Journal of Geotechnical Engineering, American Society of Civil Engineering, v. 118, no. 10, p. 1529-1543.

Xia, J., Miller, R.D., and Park, C.B., 1999, Estimation of near-surface shear-wave velocity by inversion of Rayleigh waves: *Geophysics*, v. 64, no. 3, p. 691-700.

Table 1: Average Vs at all eighty-four (84) turbine sites in Blue Canyon Phase II

Tower #	Vs (m/sec) (Top 5 m)	Vs (m/sec) (Top 10 m)	Vs (m/sec) (Top 20 m)	Vs (m/sec) (N-S Line)	Vs (m/sec) (E-W Lines)
201	744	1010	1350	1350	1429
202	843	1086	1309	1319	1242
203	853	1279	1579	1365	1629
204	880	1146	1415	1389	1564
205	891	1109	1580	1502	1523
206	781	980	1401	1320	1432
207	852	1079	1521	1541	1495
208	801	1000	1271	1327	1288
209	735	1085	1335	1339	1345
210	680	846	1158	1131	1167
211	906	1182	1507	1573	1543
212	862	1133	1392	1387	1425
213	936	1232	1533	1529	1543
214	759	1124	1399	1390	1524
215	615	921	1260	1288	1229
216	750	989	1346	1395	1326
217	839	1138	1563	1553	1630
218	895	1192	1476	1426	1511
219	823	1257	1483	1509	1592
220	834	1055	1296	1384	1303
221	728	947	1193	1184	1166
222	778	1088	1338	1335	1283
223	878	952	1153	1259	1098
224	667	915	1344	1397	1301
225	683	907	1353	1343	1378
226	844	1081	1280	1268	1243
227	669	836	1151	1232	1099
228	868	1092	1476	1520	1447
229	842	1090	1514	1620	1513
230	647	764	1088	1110	1046
231	785	1003	1296	1300	1257
232	745	948	1351	1347	1329
233	662	816	1055	890	951
234	830	1062	1314	1385	1343
235	816	1071	1506	1444	1440
236	786	995	1463	1385	1461
237	562	758	1146	1081	1193
238	809	918	1212	1189	1227
239	1364	1357	1612	1648	1700
240	665	829	1245	1161	1290
241	846	1073	1497	1435	1533
242	575	826	1197	1140	1254

Table 1: (Continued)

Tower #	Vs (m/sec) (Top 5 m)	Vs (m/sec) (Top 10 m)	Vs (m/sec) (Top 20 m)	Vs (m/sec) (N-S Line)	Vs (m/sec) (E-W Lines)
243	590	801	1041	1057	1056
244	515	741	978	947	988
245	609	823	1212	1201	1193
246	583	803	1154	1073	1174
247	679	934	1245	1223	1373
248	511	729	961	933	947
249	604	841	1120	1118	1141
250	751	1009	1411	1367	1484
251	550	765	1118	1062	1064
252	591	760	1136	1152	1094
253	560	758	1010	1030	982
254	572	739	1077	1155	1062
255	637	837	1119	1093	1123
256	672	859	1105	1085	1085
257	520	727	992	1067	923
258	489	663	892	1051	818
259	603	795	1042	1098	912
260	508	684	904	909	847
261	532	692	861	920	747
262	811	866	1027	969	1018
263	916	1092	1357	1377	1462
264	786	895	1100	1177	991
265	815	911	1239	1310	1201
266	798	1018	1311	1392	1244
267	717	868	1112	1045	1122
268	545	678	1015	1046	992
269	593	833	1119	938	1126
270	603	777	1164	1103	1079
271	650	894	1311	1213	1308
272	683	928	1280	1123	1240
273	869	1089	1556	1641	1471
274	908	1209	1718	1762	1592
275	607	812	1066	996	1096
276	774	1002	1403	1383	1388
277	751	1029	1337	1334	1359
278	765	1077	1392	1273	1596
279	928	1218	1540	1620	1565
280	653	807	1120	1268	1032
281	704	871	1311	1353	1292
282	691	870	1302	1242	1258
283	804	1212	1505	1361	1476
284	923	1199	1499	1484	1564

Table 2: Summary table of potential voids (Blue Canyon Wind Mill Farm Phase II)

Tower #	Label[1]	Location and Dimension of Potential Void[2]	Confidence Level[3]
201	L1-1	3.3 m North, 0.0-m East in 6.9-12.2 m depth and 2.3 m diameter	3
	SSA-1	2.9 m North, 1.0 m East in 2.0-10.0 m depth and 3.1 m diameter	6
202	L1-1	0.9 m South, 0.0-m East in 4.9-8.9 m depth and 2.9 m diameter	6
	L1-2	5.8 m South, 0.0-m East in 5.6-9.4 m depth and 2.8 m diameter	6
	L2-1	14.6 m North, 12.6 m West in 7.5-11.4 m depth and 2.8 m diameter	7
211	L1-1	6.8 m South, 0.0-m East in 8.2-13.1 m depth and 3.5 m diameter	8
213	L3-1	0.0 m North, 11.8 m East in 7.0-12.0 m depth and 4.4 m diameter	8
218	L2-1	14.6 m North, 1.9 m West in 7.8-12.9 m depth and 3.7 m diameter	8
220	SSA-1	2.9 m North, 5.9 m East in 2.0-10.0 m depth and 3.3 m diameter	6
222	L2-1	14.6 m North, 5.3 m West in 11.1-14.7 m depth and 3.6 m diameter	6
	L2-2	14.6 m North, 6.2 m East in 11.7-15.3 m depth and 2.4 m diameter	6
223	SSA-1	7.3 m North, 3.1 m East in 2.0-10.0 m depth and 4.3 m diameter	3
226	L1-1	2.5 m South, 0.0-m East in 6.9-12.0 m depth and 3.7 m diameter	8
	L3-1	0.0 m North, 2.3 m West in 6.7-12.6 m depth and 4.3 m diameter	7
	L3-2	0.0 m North, 7.8 m West in 11.5-16.5 m depth and 3.7 m diameter	6
228	L2-1	14.6 m North, 2.6 m East in 12.0-18.3 m depth and 4.7 m diameter	8
	L4-1	14.6 m South, 8.0 m West in 15.4-21.0 m depth and 3.9 m diameter	7
229	L3-1	0.0 m North, 11.2 m West in 10.5-16.2 m depth and 3.5 m diameter	7
	L4-1	14.6 m South, 9.4 m West in 7.0-10.8 m depth and 6.3 m diameter	8
230	L2-1	14.6 m North, 3.8 m West in 8.7-14.4 m depth and 3.0 m diameter	5
232	SSA-1	8.3 m North, 4.4 m East in 2.0-10.0 m depth and 4.2 m diameter	7
234	L2-1	14.6 m North, 1.0 m West in 6.0-10.6 m depth and 3.7 m diameter	7
235	L1-1	2.5 m South, 0.0-m East in 11.9-17.7 m depth and 5.2 m diameter	7
239	SSA-1	7.3 m South, 1.8 m East in 2.0-10.0 m depth and 4.4 m diameter	3
240	SSA-1	6.5 m South, 5.3 m West in 2.0-10.0 m depth and 3.7 m diameter	3
242	L1-1	12.7 m South, 0.0-m East in 10.1-13.9 m depth and 2.4 m diameter	7
	L4-1	14.6 m South, 12.8 m East in 16.6-21.7 m depth and 3.4 m diameter	5
246	L1-1	10.9 m South, 0.0-m East in 11.1-18.6 m depth and 4.9 m diameter	5
	L1-2	2.1 m South, 0.0-m East in 13.3-18.9 m depth and 3.6 m diameter	3
247	SSA-1	14.0 m South, 12.4 m East in 2.0-10.0 m depth and 3.7 m diameter	6
248	L2-1	14.6 m North, 4.8 m East in 6.8-12.1 m depth and 2.7 m diameter	5
	SSA-1	1.7 m South, 3.8 m East in 2.0-10.0 m depth and 2.7 m diameter	6
251	SSA-1	0.7 m North, 7.9 m East in 2.0-10.0 m depth and 3.4 m diameter	6
	L2-1	14.6 m North, 2.6 m West in 11.3-15.6 m depth and 1.8 m diameter	4
252	L4-1	14.6 m South, 3.8 m West in 8.2-14.0 m depth and 2.6 m diameter	5
254	SSA-1	14.3 m South, 5.4 m East in 2.0-10.0 m depth and 3.7 m diameter	6
255	L3-1	0.0 m North, 5.6 m West in 11.4-17.2 m depth and 3.4 m diameter	8
	L3-2	0.0 m North, 4.3 m East in 10.5-16.4 m depth and 2.7 m diameter	8
257	SSA-1	3.1 m North, 5.6 m East in 2.0-10.0 m depth and 4.6 m diameter	2
258	SSA-1	9.1 m North, 3.7 m East in 2.0-10.0 m depth and 8.2 m diameter	2
259	SSA-1	13.6 m South, 6.7 m East in 2.0-10.0 m depth and 5.6 m diameter	4
260	SSA-1	4.0 m South, 13.8 m East in 2.0-10.0 m depth and 3.3 m diameter	6

Table 2: (Continued)

	L1-1	3.2 m North, 0.0-m East in 10.4-15.8 m depth and 2.5 m diameter	2
262	SSA-1	15.0 m South 15.0 m East in 2.0-10.0 m depth and 4.3 m diameter	6
	L1-1	10.6 m South, 0.0-m East in 9.7-16.9 m depth and 3.5 m diameter	6
	L3-1	0.0 m North, 5.3 m East in 4.2-9.1 m depth and 3.6 m diameter	2
	L4-1	14.6 m South, 10.8 m East in 15.2-21.6 m depth and 4.7 m diameter	2
263	L3-1	0.0 m North, 9.4 m East in 9.9-15.9 m depth and 2.7 m diameter	2
264	SSA-1	13.1 m North, 3.0 m East in 2.0-10.0 m depth and 4.2 m diameter	3
265	SSA-1	6.1 m North, 1.7 m East in 2.0-10.0 m depth and 5.7 m diameter	2
	SSA-2	5.8 m North, 10.7 m East in 2.0-10.0 m depth and 5.6 m diameter	2
	L4-1	14.4 m South, 9.2 m East in 8.6-20.3 m depth and 3.0 m diameter	2
267	SSA-1	13.5 m North, 7.9 m East in 2.0-10.0 m depth and 5.6 m diameter	6
	SSA-2	3.4 m South, 2.9 m East in 2.0-10.0 m depth and 4.2 m diameter	3
270	L4-1	14.6 m South, 3.2 m West in 12.2-17.3 m depth and 4.3 m diameter	6
271	L1-1	5.5 m South, 0.0-m East in 8.4-12.9 m depth and 2.4 m diameter	7
	SSA-1	7.4 m North, 9.9 m East in 2.0-10.0 m depth and 4.5 m diameter	6
	SSA-2	7.3 m South, 5.3 m East in 2.0-10.0 m depth and 4.2 m diameter	6
275	L1-1	11.8 m South, 0.0-m East in 8.5-14.0 m depth and 2.8 m diameter	6
	L1-2	12.3 m North, 0.0-m East in 6.7-10.9 m depth and 2.6 m diameter	6
	L2-1	14.6 m North, 3.2 m West in 8.0-13.2 m depth and 2.6 m diameter	6
276	L4-1	14.6 m South, 10.5 m East in 11.0-15.2 m depth and 4.3 m diameter	5
277	L4-1	14.6 m South, 1.4 m West in 7.1-11.6 m depth and 2.3 m diameter	5
278	SSA-1	2.2 m North, 3.3 m East in 2.0-10.0 m depth and 4.2 m diameter	4
280	L2-1	14.6 m North, 12.5 m West in 6.5-11.9 m depth and 2.9 m diameter	7
281	SSA-1	13.9 m North, 11.3 m East in 2.0-10.0 m depth and 3.4 m diameter	5
283	L3-1	0.0 m North, 0.6 m West in 5.9-10.3 m depth and 2.2 m diameter	5
	L4-1	14.6 m South, 9.8 m West in 5.5-10.0 m depth and 4.1 m diameter	6
	SSA-1	6.6 m South, 10.4 m East in 2.0-10.0 m depth and 3.8 m diameter	6

[1] Name marked on the reported maps of 2-D Vs, side scattering analysis (SSA), and surface-wave imaging by attenuation (SIA).
[2] Location from the center of the tower and maximum dimension possible.
[3] Confidence level of interpretation: 0=No confidence, 10=Absolute confidence.

Table 3: Sites where one or more lines were adjusted to a shorter length due to terrain conditions.

Tower #	Line 1	Line 2	Line 3	Line 4
208		√	√	√
220	√	√	√	N/A
222			√	
227			√	√
232	√	√	√	
234			√	√
237		√	√	√
241				√
248	√	√	√	√
250	√			
251	√	√	√	√
259			√	√
265	√			
271	√	√	√	√
275				√
277				√

√: Lines with a shorter receiver spacing of 2 ft to account for a narrow space available
N/A: Data not acquired due to terrain condition

Table 4: Optimum acquisition parameters—Rules of thumb

Material Type* (V_s in m/sec)	x_1 (m)	dx (m)	x_M (m)	Optimum Geophone (Hz)	Optimum Source+ (Kg)	Recording Time (ms)	Sampling Interval (ms)
Very Soft ($V_s < 100$)	1 – 5	0.25 – 0.5	≤ 20	4.5	≥ 5.0	2000	1.0
Soft ($100 < V_s < 300$)	5 – 10	0.5 – 1.0	≤ 30	4.5	≥ 5.0	2000	1.0
Hard ($200 < V_s < 500$)	10 – 20	1.0 – 2.0	≤ 50	4.5 – 10.0	≥ 5.0	1000	0.5
Very Hard ($500 < V_s$)	20 – 40	2.0 – 5.0	≤ 100	4.5 – 40.0	≥ 5.0	1000	0.5

* Average properties within about 30-m depth range.
+ Weight of sledgehammer.

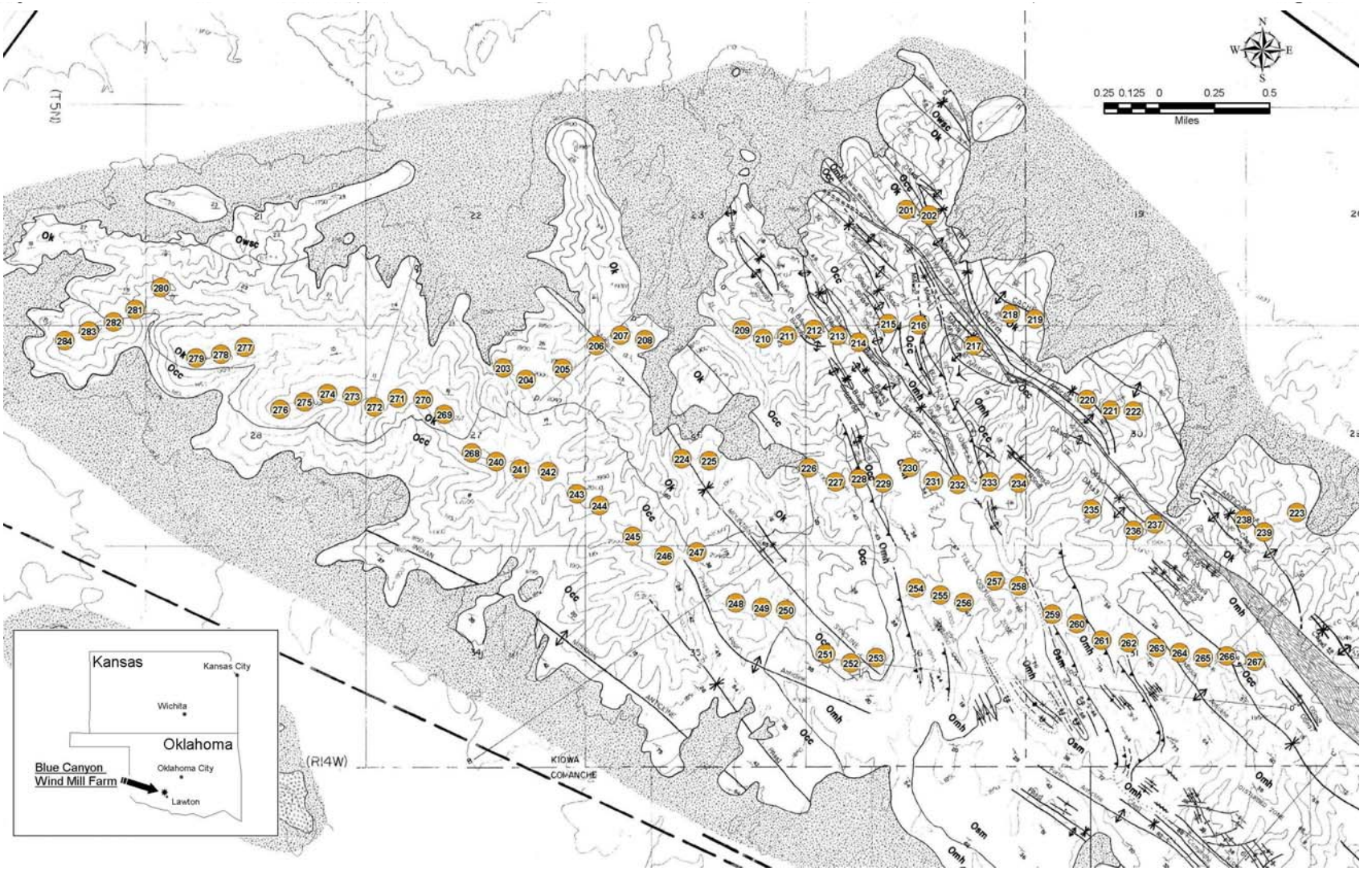

Figure 1. Location and geologic map of all eighty four (84) turbine sites to be constructed during the second phase of wind mill farm in the Blue Canyon Wind Mill Farm near Lawton, Oklahoma (inset).

Figure 2. Photos showing typical terrain conditions in the project area at the Blue Canyon Wind Mill Farm near Lawton, Oklahoma.

- Four (4) seismic lines: Lines 1-4
- Station spacing: 1.22 m (4 ft)
- Receivers: 4.5-Hz geophones
- Recording: 48-channel (2 of 24-channel Geometrics Geode)
- Source: 16-lb sledgehammer (3-impact stack)
- Recording: 1-sec recording time with 1-ms sampling interval
- Shot interval: 1 station
- Number of shots: 24 shots per line
- 2-D shear-velocity (Vs) imaging: all 4 lines
- Side scattering analysis (SSA): lines 2 and 4
- Surface-wave imaging by attenuation (SIA): all 4 lines

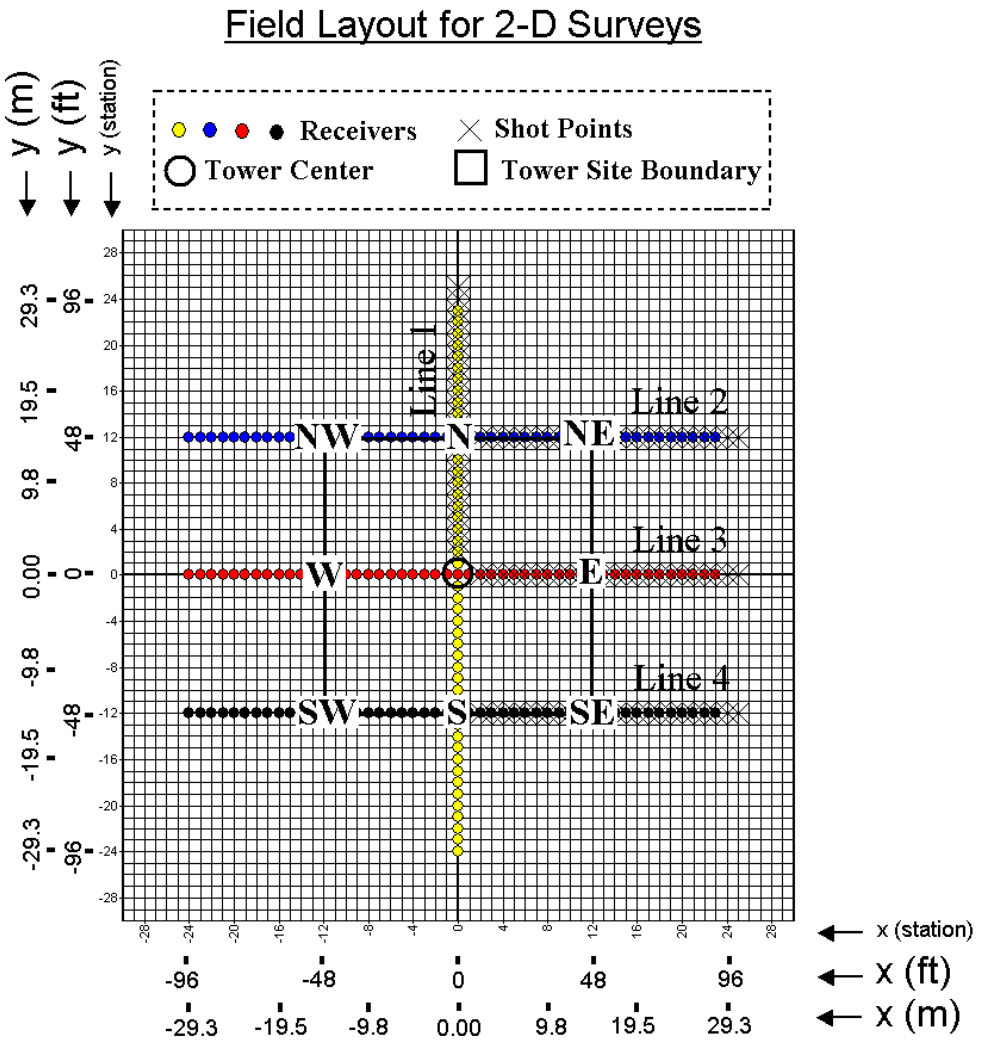

Figure 3. A schematic showing the field logistics used for the 2-D surveys. Summary of acquisition parameters is listed on top.

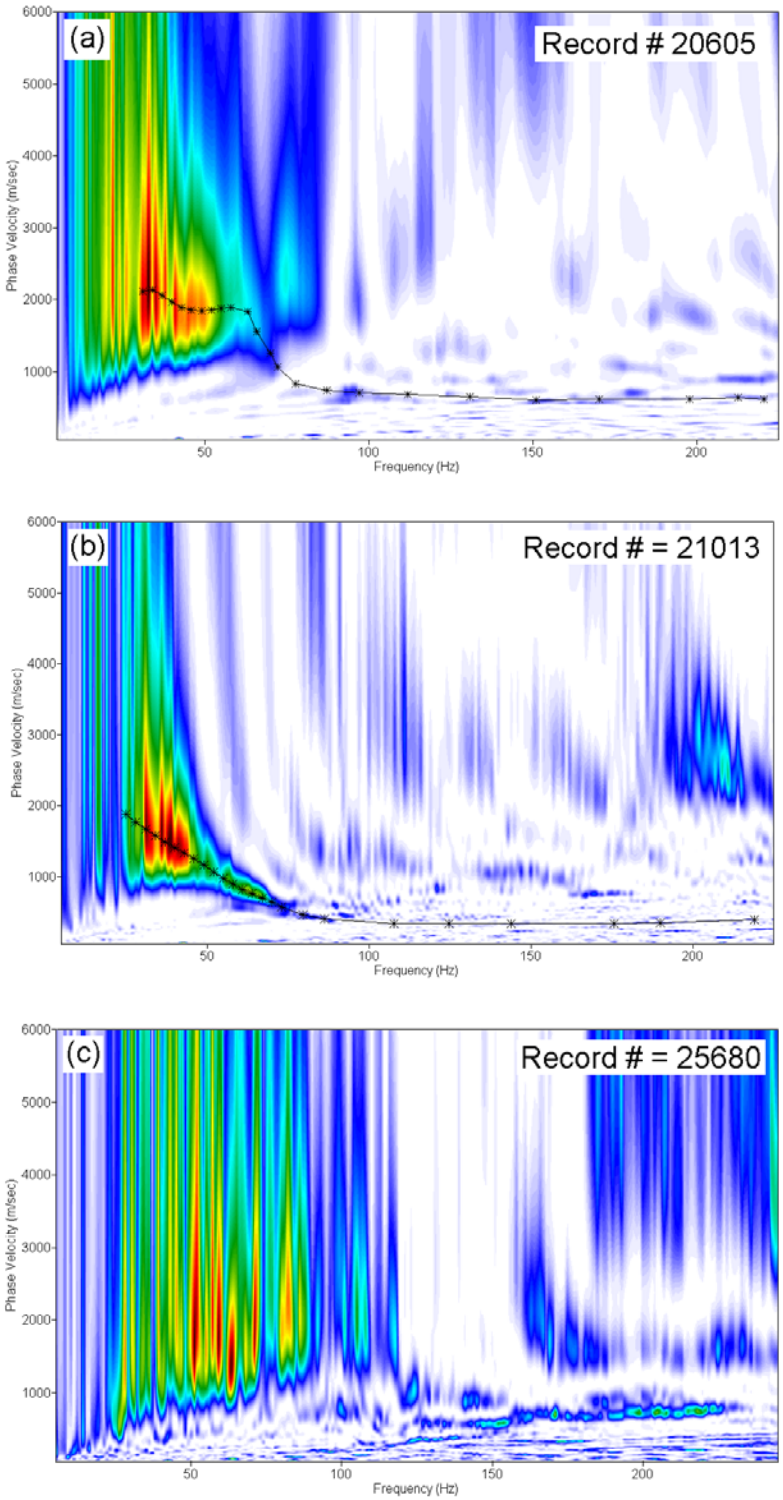

Figure 4. Quality of seismic data collected in the project area as judged from the dispersion image: (a) typical quality constituting more than ninety percent (90%) of total data, (b) extraordinary quality (≈ 5%), and (c) poor quality (≈ 5%) that was discarded during the construction of the 2-D Vs maps.

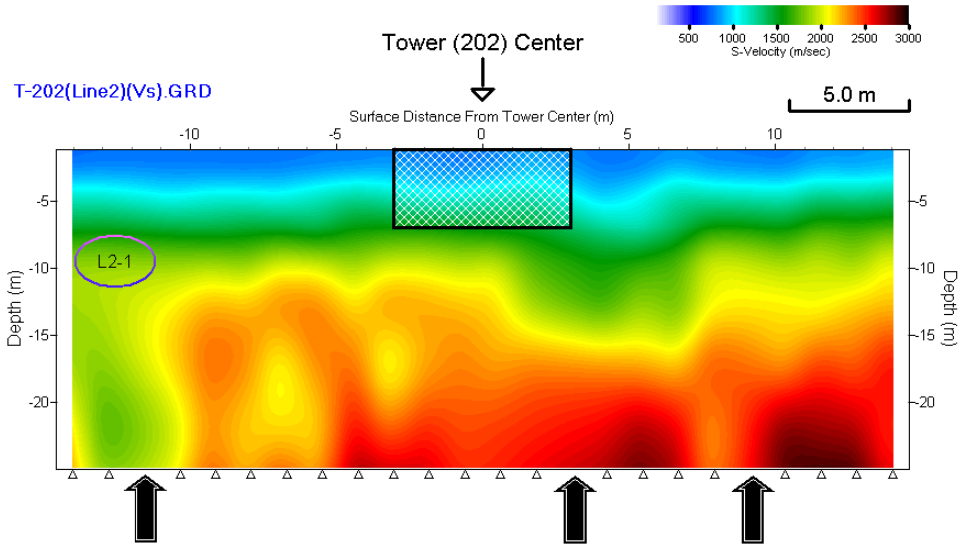

Figure 5. A 2-D Vs map showing some surface points (marked by three upright arrows) where the corresponding seismic records were discarded from the construction process of the map because of data quality too low to be analyzed. Points marked by small triangles at the bottom indicate surface coordinates of the 1-D (ten-layer) Vs profiles used for the construction of the map through a gridding algorithm.

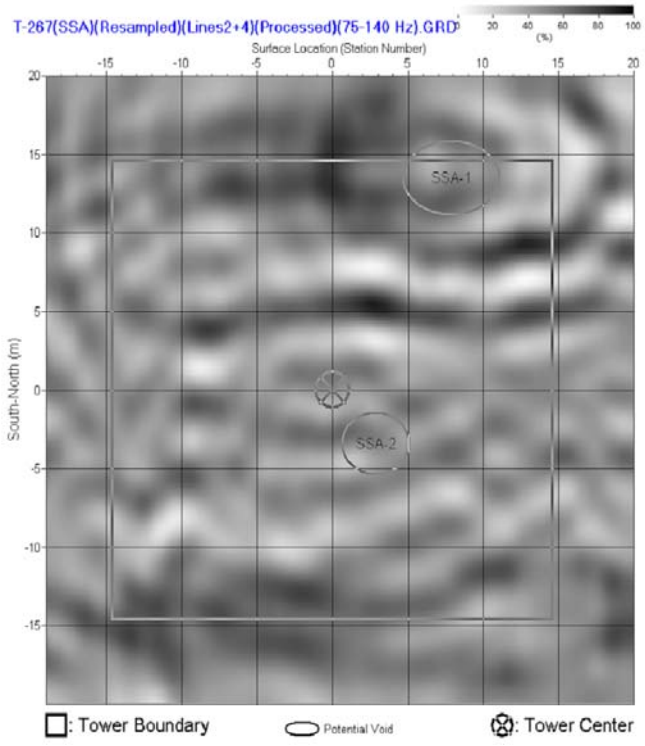

Figure 6. An SSA map constructed from the records of lines 2 and 4 acquired at T-267. An artificial grid of (±) 20 m by (±) 20 m size was used with an interval of 0.2 m.

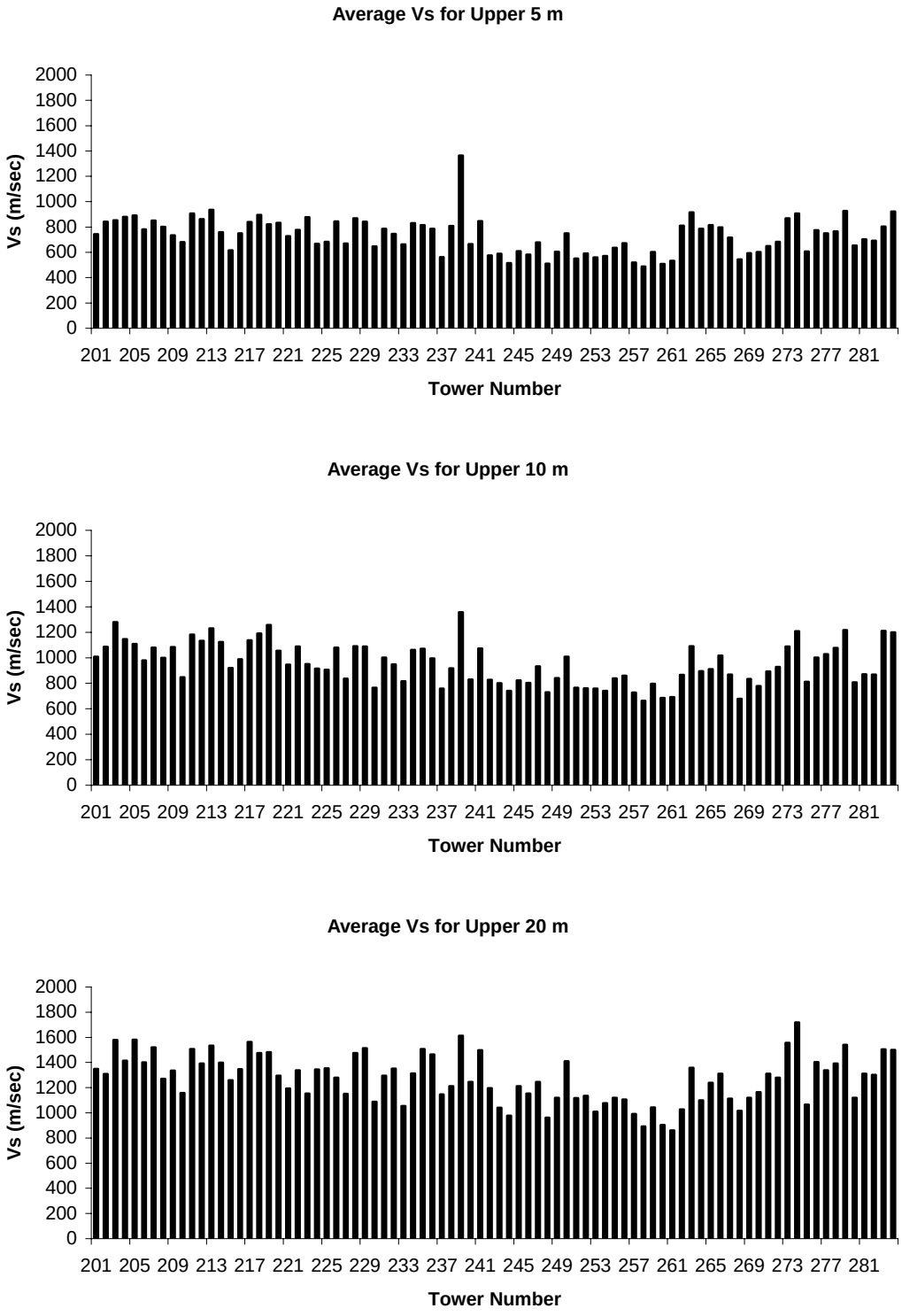

Figure 7. Average Vs calculated for top 5 m, 10 m, and 20 m depth ranges at all eighty-four (84) sites. Average Vs values from N-S line (line 1) and E-W lines (lines 2-4) are also displayed.

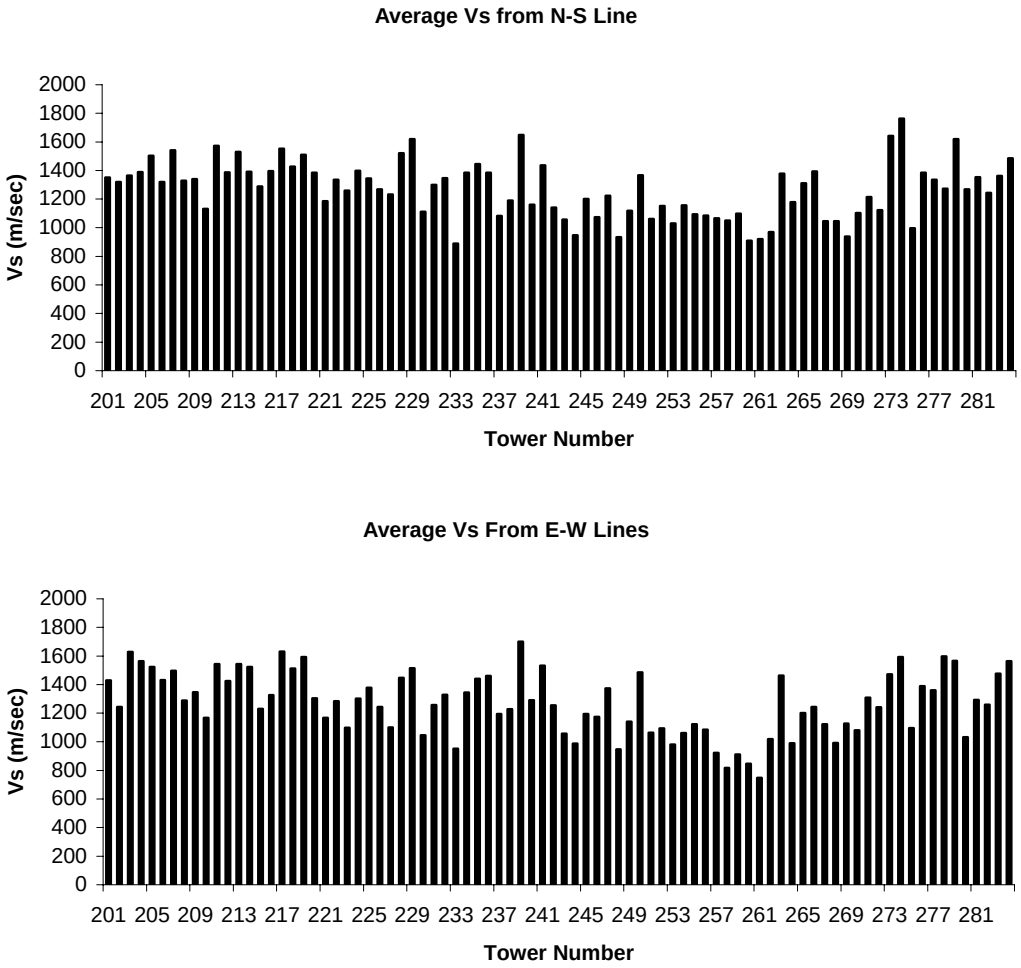

Figure 7. (Continued)

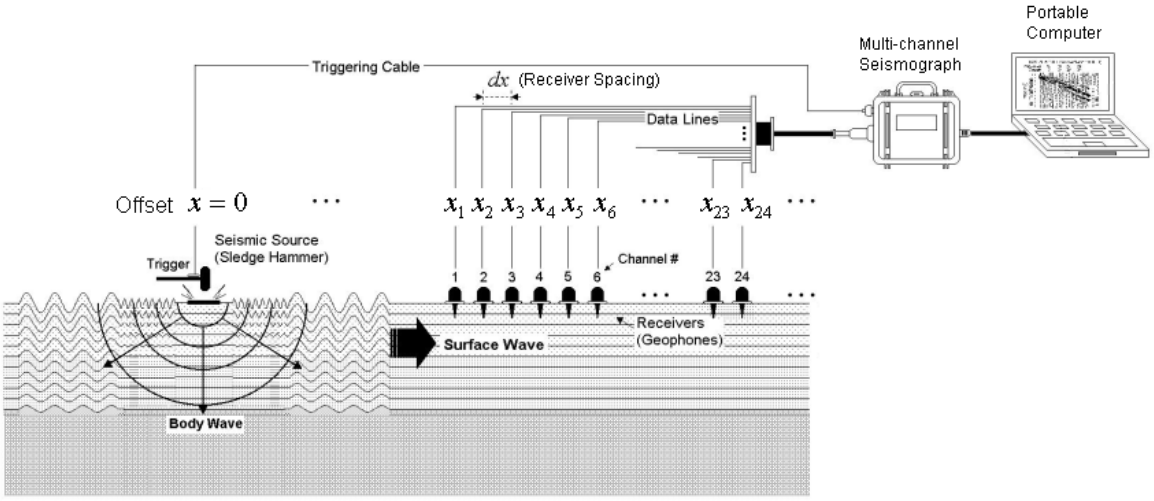

Figure 8. A schematic of a typical MASW configuration.

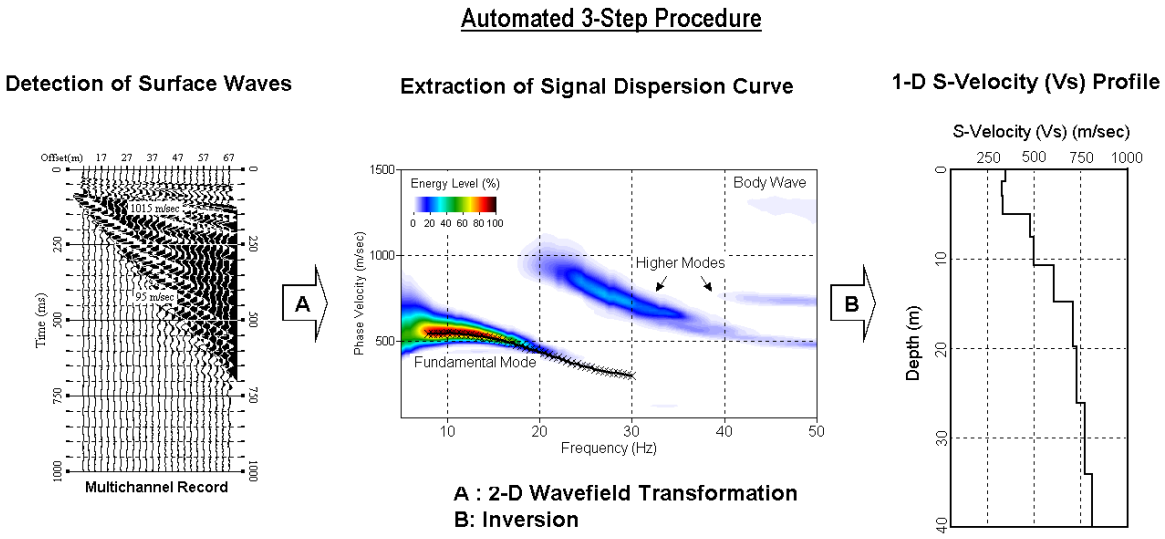

Figure 9. A 3-step scheme for MASW data processing illustrated by an actual field data set acquired near Yuma, Arizona.

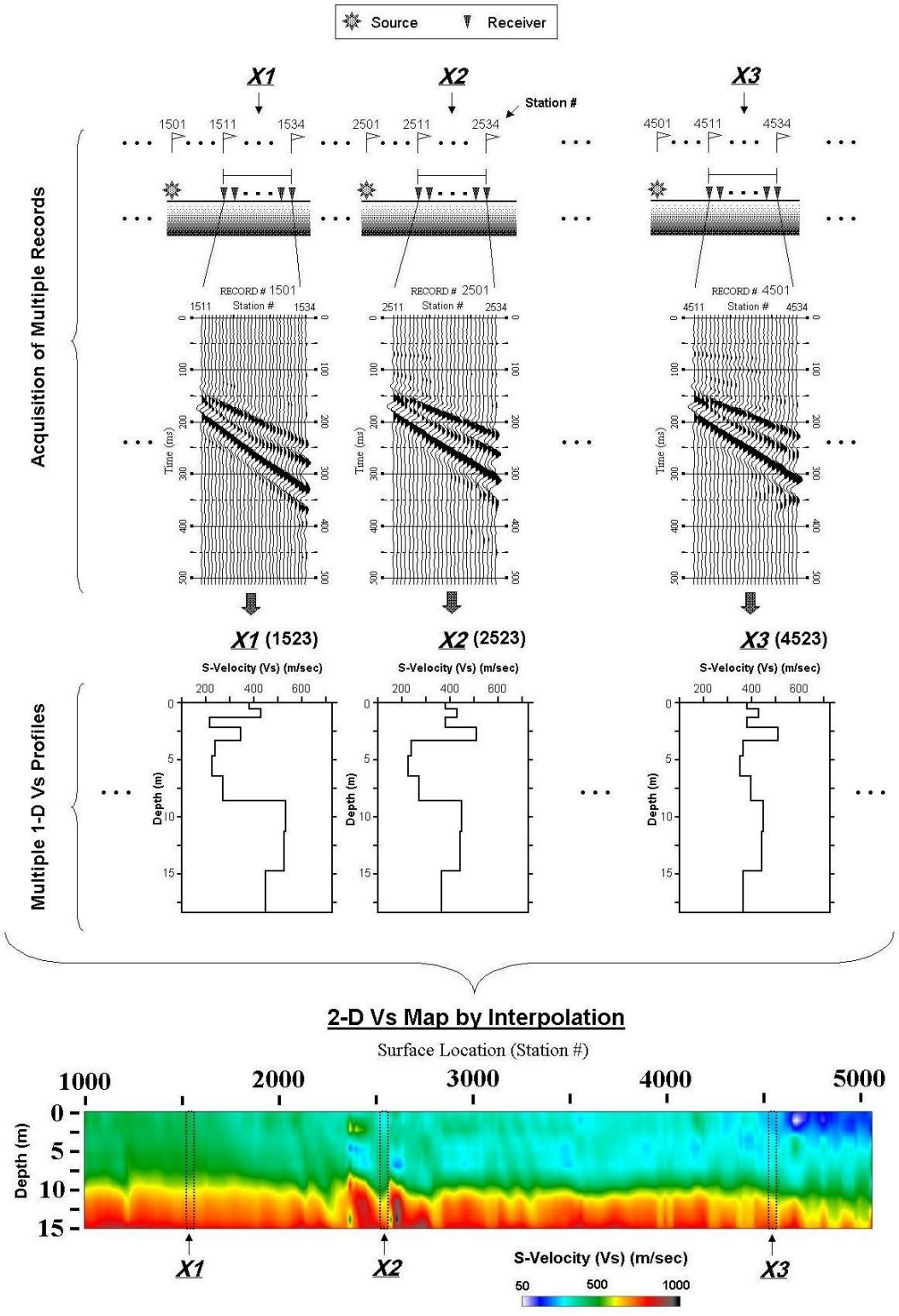

Figure 10. Overall procedure to construct a 2-D Vs map from the MASW survey.

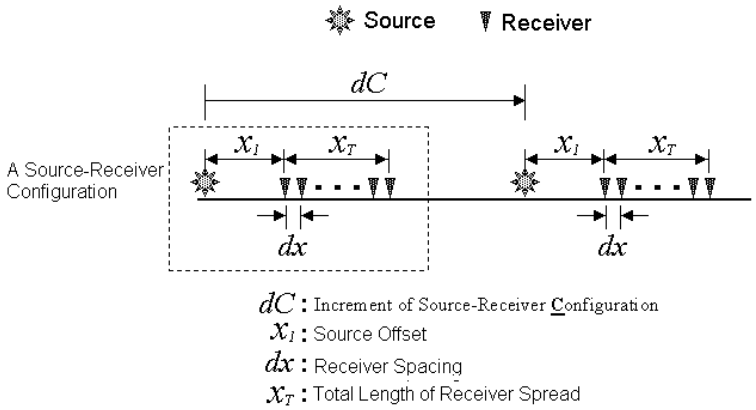

Figure 11. A source-receiver configuration and an increment of the configuration.

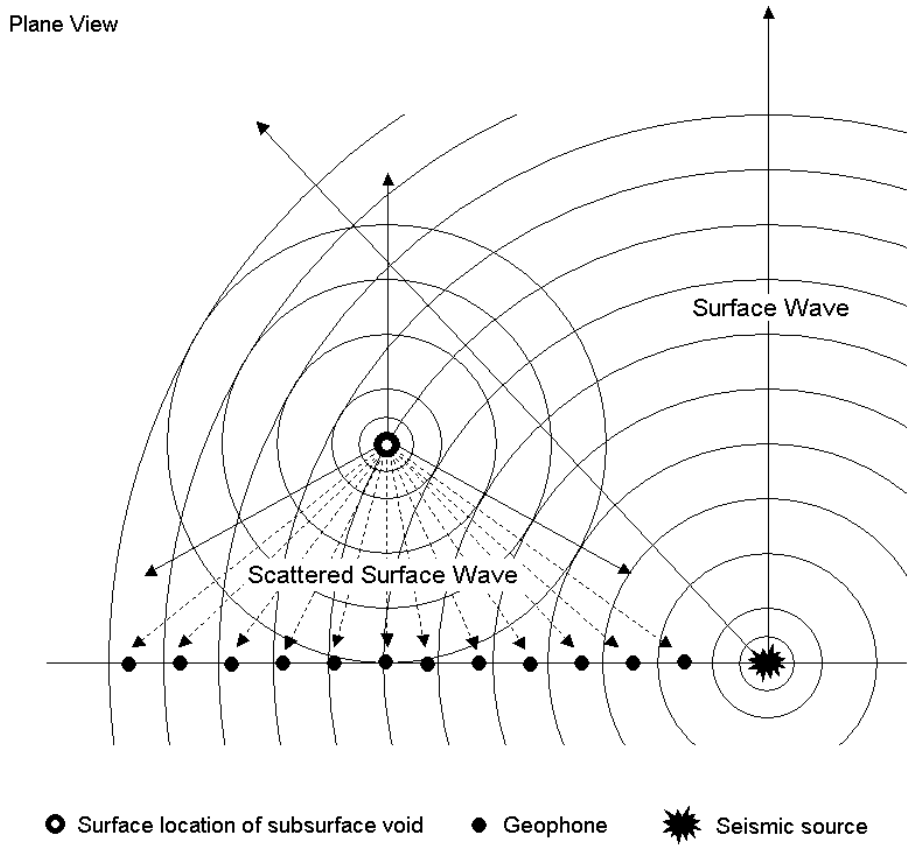

Figure 12. A plane-view schematic illustrating the scattered surface-wave generation that can be set off by a near-surface anomaly like a void.

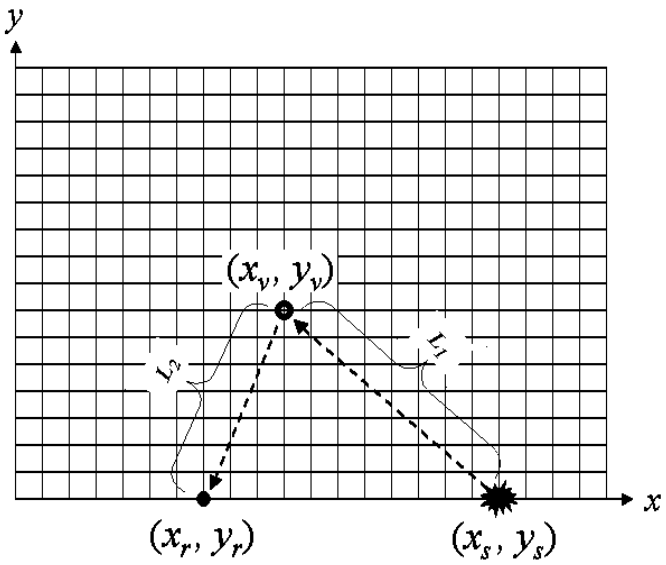

Figure 13. A fictitious grid net is used during the SSA processing in which each point (x_v, y_v) in the net is assumed as a possible scattering source of surface waves generated by a source at (x_s, y_s). Then, a receiver at (x_r, y_r) can record such scattered waves.

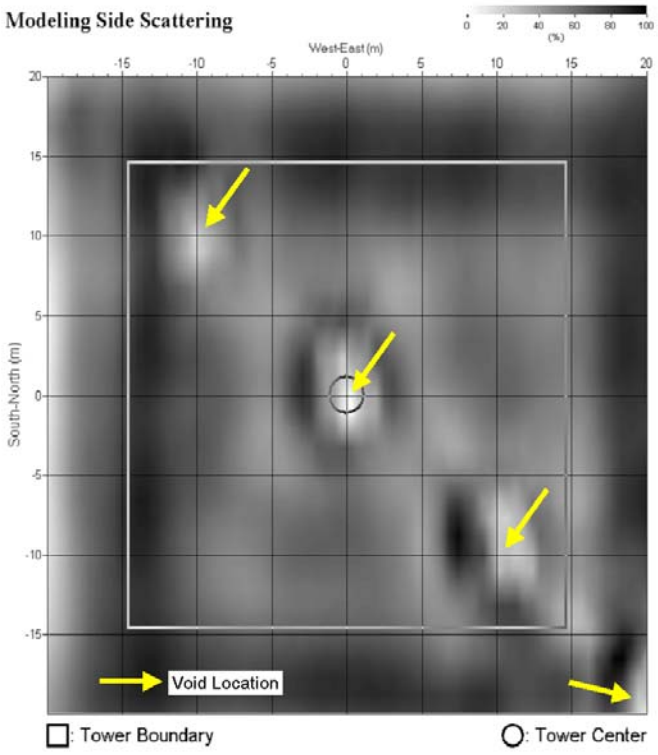

Figure 14. An SSA map from modeling. Four (4) voids were modeled below the marked surface points with a spherical diameter (D) and a depth (Z) of (D=1m, Z=1m), (D=2m, Z=2m), (D=2m, Z=3m), and (D=1m, Z=3m) from top to bottom.

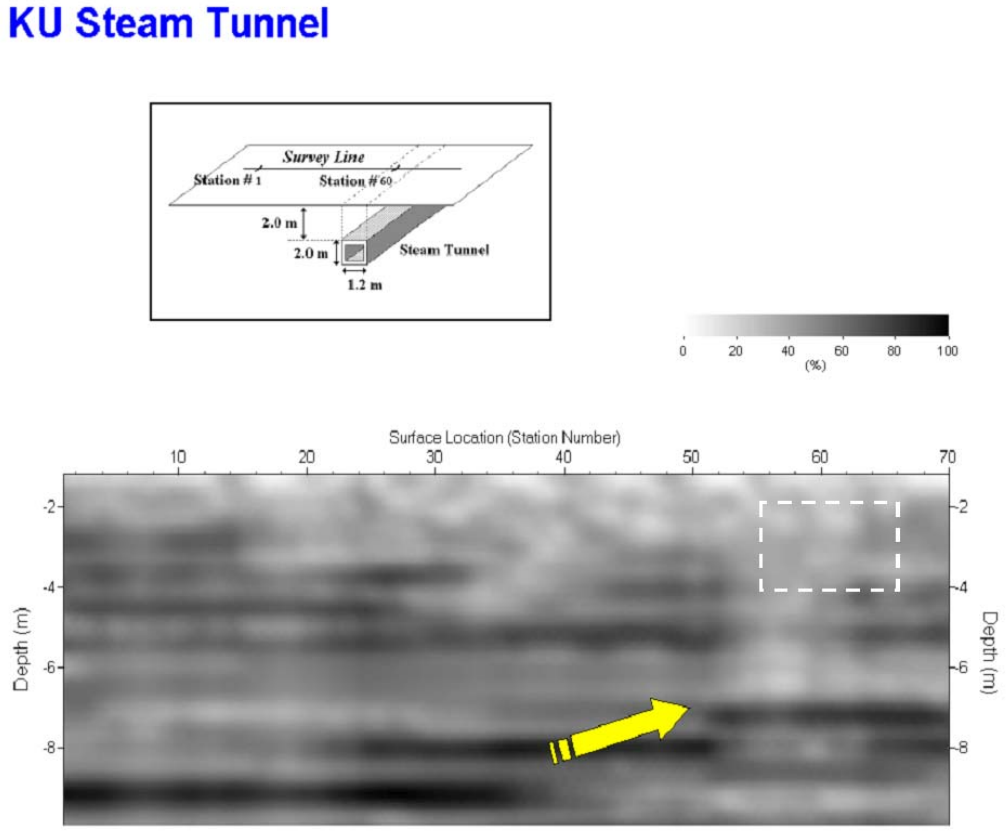

Figure 15. An SIA map constructed after an actual field survey at a soccer field on the campus of the University of Kansas (KU), Lawrence, Kansas. Actual location and dimension of the tunnel is marked on the map.